Title

Structure Functions: Their Status and Implications

Author

Hinchliffe, I

Publication Date

1988-09-01

LBL-25820

Lawrence Berkeley Laboratory
UNIVERSITY OF CALIFORNIA

Physics Division

Invited talk presented at the 1988 Division of Particles and Fields Meeting, Storrs, CT, August 15–18, 1988

Structure Functions: Their Status and Implications

I. Hinchliffe

September 1988

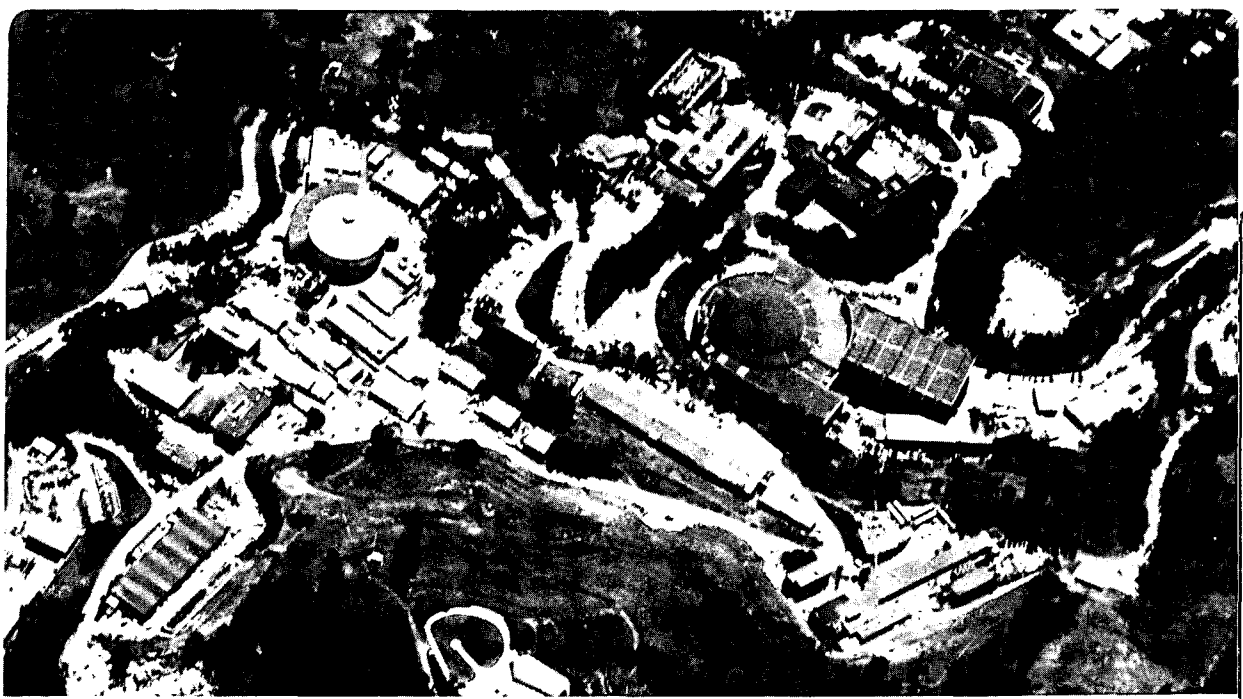

Prepared for the U.S. Department of Energy under Contract Number DE-AC03-76SF00098.

DISCLAIMER

September 29, 1988 LBL-25820

Structure Functions: their status and implications. *

Ian Hinchliffe

Lawrence Berkeley Laboratory
University of California
1 Cyclotron Road
Berkeley, California 94720

Invited talk given at the 1988 Division of Particles and Fields meeting, Storrs, Connecticut, August 15–18, 1988.

Abstract

I discuss the current status of structure functions. Attention is given to the uncertainties in them and the implications of these uncertainties for experimental predictions. I indicate which experiments are capable of removing these uncertainties.

*This work was supported by the Director, Office of Energy Research, Office of High Energy and Nuclear Physics, Division of High Energy Physics of the U.S. Department of Energy under Contract DE-AC03-76SF00098.

Knowledge of the parton distribution functions is needed in order to predict event rates for processes that involve a hadron in the initial state and that have a large momentum transfer. Examples include the production of heavy quarks in ep or $p\bar{p}$ interactions and the production of jets or W and Z bosons at the Tevatron or $Sp\bar{p}S$ colliders. In this talk, I will first remind you how the parton distribution functions are extracted from data on deep inelastic scattering.[1)] I will emphasize the interplay between the definition of the distribution functions and the form of the partonic hard scattering cross-section. The regions of x and Q^2 which are important but which cannot be probed directly at present will be discussed. I will then discuss some applications of these distribution functions to hadron–hadron collisions. I will contrast the uncertainties in predicted rates due to the distribution functions with those due to higher order corrections and ambiguities in the choice of partonic hard scattering scales. Finally, I will indicate what experiments in the near future can help resolve the remaining uncertainties.

I will not discuss the recent controversy surrounding the structure function of a polarized proton.[2)] This is discussed elsewhere at this meeting.[3)] Neither, will I discuss the nuclear A dependence of deep inelastic scattering.[4)]

1. Parton Distribution Functions, their definition and measurement.

I will begin with brief review of the parton model, mainly to establish notation. More details can be found a review article[1] where a complete set of references may also be found. The kinematics of deep inelastic scattering the differential cross–section may be written as

$$\frac{d\sigma}{dxdy} = \frac{4\pi\alpha_{em}^2 s}{Q^4}\left[\frac{1+(1-y)^2}{2}2xF_1(x,Q^2) + (1-y)(F_2(x,Q^2) - 2xF_1(x,Q^2))\right] \tag{1}$$

The variables are defined as follows (see Figure 1): q is the momentum of the exchanged photon and p is the momentum of the target proton and k is that of the incoming electron

$$Q^2 = -q^2; \nu = \frac{q\cdot p}{m_p}; x = \frac{Q^2}{2m_p\nu}; y = \frac{q\cdot p}{k\cdot p}; s = 2p\cdot k + m_p^2 \tag{2}$$

where m_p is the proton mass.

In the parton model we have,

$$2xF_1 = F_2 = \sum_i \int_x^1 dy q_i(y) \hat{\sigma}(\frac{x}{y}). \tag{3}$$

I have included only photon exchange (see figure 1) for simplicity. At very high Q^2 which is accessible at HERA[5] one must include Z exchange also. The parton distribution function of parton of type i carrying fraction x of the protons momentum has been introduced ($q_i(x)$). Here $\hat{\sigma}$ can be thought of as the cross-section for the process $\gamma + q \rightarrow anything$. At lowest order in α_s, the strong coupling constant, the process is simply $\gamma + q \rightarrow q$ and we have

$$\hat{\sigma}_i(z) = e_i^2 \delta(z-1) \tag{4}$$

Here e_i is the electric charge of quark of type: The δ–function simply enforces the requirement that the final quark be on mass shell and is massless. If we consider the partonic process to order α_s, there are now two possible final states: q which arises from a virtual correction to the lowest order process and $q + g$ (here g denotes a gluon) which arises from $\gamma + q \rightarrow q + g$; $\hat{\sigma}$ now takes the form

$$\hat{\sigma}_i(z) = \left[e_i^2 \sigma(z-1) + \sigma_i(z, Q^2) \right] \tag{5}$$

where

$$\sigma_i(z, Q^2) = \frac{\alpha_s}{2\pi} e_i^2 \left[t P_{qq}(z) + f(z) + 0\left(\frac{1}{Q^2}\right) \right] \tag{6}$$

with

$$P_{qq}(z) = \frac{4}{3} \frac{(1+z^2)}{1-z}. \tag{7}$$

Here $t = \log(Q^2/\mu^2)$. The scale μ has been introduced. It arises as an infrared cut off. In deriving equation (5) it is necessary to integrate over the angle between the incoming quark and outgoing gluon (θ). This integral has the form

$$\int \frac{d(\cos\theta)}{1 - \cos\theta} \tag{8}$$

and is singular when $\theta \to 0$, a collinear singularity. If the quark had a mass μ, this integral would have the form

$$\int \frac{d(\cos\theta)}{1-\cos\theta+\mu^2/Q^2} \tag{9}$$

and would give rise to the $\log(Q^2/\mu^2)$ term. The presence of this large log ruins the expansion is α_s since the next order will contain a term of order $t^2\alpha_s^2$. This dangerous term can be absorbed into the definition of the distribution function viz,

$$q_i(x,t) = q_i(x) + \frac{\alpha_s t}{2\pi}\int_x^1 \frac{dy}{y} q(y) P_{qq}\left(\frac{x}{y}\right). \tag{10}$$

Then

$$F_1 = \sum_i \int_x^1 e_i^2 \frac{dy}{y} q_i(y,Q^2)\hat{\sigma}\left(\frac{x}{y}\right) \tag{11}$$

where now

$$\hat{\sigma}(z) = e_i^2\left(\delta(z-1) + \frac{\alpha_s}{2\pi} f(z)\right) \tag{12}$$

In practice the problem is more complicated, since at order α_s gluons can enter in the initial state via the process $g+\gamma \to q+\bar{q}$. Equation 10 is replaced by*

$$q_i(x,Q^2) = q_i(x) + \frac{\alpha_s}{2\pi} t \int_x^1 \left(q_i(y)P_{qq}(\frac{x}{y}) + g(y)P_{gq}(\frac{x}{y})\right)\frac{dy}{y}. \tag{13}$$

All partonic process have the same collinear divergences and hence all can have their rates written in terms of $q_i(x,Q^2)$ with no remaining divergences. This miracle is known as factorization[7] and guarantees that all partonic processes are computable in terms of the same set of parton distribution functions.

It is important to realize that there is some arbitrariness is what is defined to be $q_i(x,Q^2)$ and what is $\hat{\sigma}(z)$. If the definition of $q_i(x,Q^2)$ in equation 11 were replaced by

$$q_i(x,Q^2) = q_i(x) + \frac{\alpha_s}{2\pi}\int_\pi^1 \frac{dy}{y} q_i(y)\left[tP_{qq}(\frac{x}{y}) + f(\frac{x}{y})\right] \tag{14}$$

*This equation will look more familiar in the standard Altarelli-Parisi[6] form

$$\frac{dq(x,Q^2)}{d\log Q^2} = \frac{\alpha_s(Q^2)}{2\pi}\int_x^1 \frac{dy}{y}\left[q(y,Q^2)P_{qq}(\frac{x}{y}) + g(y,Q^2)P_{gq}(\frac{x}{y})\right]$$

then $\hat{\sigma}(z)$ equation 12 would become

$$\hat{\sigma}(z) = e_i^2 \delta(z-1). \tag{15}$$

It is important when processes are computed to next to leading order (NLO) in α_s that this scheme dependence be kept in mind. The same scheme must be used for all processes.

Notice that the gluons only enter the formula for F_2 indirectly via equation 13. The gluon distribution ($g(x,Q^2)$) can only be determined from the growth in the antiquarks with Q^2, its value is therefore correlated with that of α_s.

2. Data Sets

In principle, many partonic processes can be used to determine the distribution functions. In practice, however, the main source of information is from deep inelastic scattering which can be used to determine the quark distributions quite accurately. In the case of the gluon distribution, other data (discussed below) can provide valuable information. I shall begin with a survey of the deep–inelastic scattering data[8] and will comment on the other processes below.

Data on deep inelastic scattering are available from scattering of electrons (SLAC[9] experiments), muons (BCDMS,[10,11] EMC,[12] BFP[13]), and neutrinos (CHARM,[14] CCFRR,[15] CDHS,[16,17] BEBC[18]) from various targets. Different combinations of cross–sections enable the distributions of the different quark flavors in a proton to be extracted. For example, the production of charm in neutrino scattering proceeds via the Cabbibo allowed (suppressed) process $\nu + s(d) \rightarrow \mu^- + c$ and a measurement of this enables the strange quark distribution to be extracted. Data on protons (Hydrogen) and neutrons (bound in Deuterium) must be used to separate the up and down quark distributions in a proton. Many of the data have very small statistical errors, but there are large systematic differences. This problem is illustrated in figure 2 which shows a comparison of $F_2(x,Q^2)$ as measured by EMC,[12] BCDMS[11] and SLAC[9] data on a hydrogen target. The EMC and BCDMS experiments cover the same kinematic range but do not agree. BCDMS is higher at small x and lower at large

x than EMC. The ratio of them is approximately independent of Q^2. It is not clear which of these data provides a better extrapolation of the SLAC data into the range of larger Q^2. A comparison of the EMC[12] data on an iron target with the BCDMS[19] data on carbon reveals similar systematic differences.

In the case of measurements on an isoscalar target there is a relationship between $F_2^{\mu N}$ and $F_2^{\nu N}$. The quantity

$$R_1 = 5F_2^{\mu N}(1+a)/18F_2^{\nu} \tag{16}$$

is expected to be equal to one. The term a is due to strange quarks and is small. The CCFRR[15] and CDHS[16,17] neutrino data on an iron target when compared to the BCDMS data on carbon yield an R_1 consistent with 1. However the EMC[12] and CCFRR[15] data, both on iron targets, yield an R_1 approximately independent of x with an average value of $R_1 = .923 \pm .005$.[18] (See figure 3). These comparisons would indicate that the a more consistent picture would emerge at moderate values of x $(.2 - .5)$, if the EMC data were renormalized upwards. They would then agree with the BCDMS data in this region also. But at larger x no such simple fix is available since the EMC data are larger than BCDMS for $x \gtrsim 0.6$.

The most accurate data are on F_2; unfortunately a fit to these data gives simultaneously a value of α_s and the gluon distribution. Ideally one would like to first determine α_s from a non–singlet distribution where the gluons do not enter (such as F_3 in neutrino scattering) or from another process entirely. Errors are so large that this is not practicable†.

There are corrections of order $1/Q^2$ to the evolution of the distribution functions with Q^2 in addition to higher order (α_s^2) terms in the Altarelli–Parisi equations (Eq. 13). These higher twist $(1/Q^2)$ terms are not calculable. Their effect can be minimized by taking only data with $Q^2 > Q^2_{min}$. If the resulting value of α_s is independent of Q^2_{min}, one can have confidence that the higher twist and higher order α_s terms are negligible. Figure 4 shows the extracted

† For a review of the determination of α_s from a wide variety of processes see ref. 20

value of $\alpha_s(Q^2 = 5\ GeV^2)$ from a fit to the EMC,[12] BCDMS (Fe targets) and BPF (C target) data as a function of Q^2_{min}.[21] This figure shows that results using lowest order QCD are not stable, but that when the α_s^2 terms are included the situation improves. This figure gives some confidence that the higher twist terms are really negligible.

Existing data do not extend below $x \sim 0.01$ and cover a very small range of Q^2 at small x. This is a potential problem since for some applications it is necessary to know the parton distributions in this region. It is traditional to assume that the gluon distribution obeys

$$\lim_{x\to 0} xg(x, Q_0^2) = const. \tag{17}$$

However this form is unstable. When evolved to higher Q^2, it develops rapidly into a steeper form (see figure 5). At very small x and large Q^2, it is possible to solve the Altarelli–Parisi equations analytically. At order α_s we have

$$xg(x, Q^2) \sim e^{\sqrt{\frac{48}{(11-2n_f/3)}\log(1/x)\log\log(q^2)}} \tag{18}$$

This form is singular as $x \to 0$. It is also possible to sum to all orders in α_s the most singular terms at small x and large Q^2. This gives[22]

$$xg(x, Q^2) \sim x^{-\delta}$$

where, $\delta = 12\alpha_s \log(2)/\pi$, which is an even more singular form. It has been suggested[22] that one should use a form for $xg(x, Q_0^2)$ which is more like the asymptotic form.

$$xg(x, Q_0^2) \sim 1/\sqrt{x} \tag{19}$$

is most commonly used. It is not clear that this form is a better assumption that the conventional one, or below what value of x Eq. 17 or 19 should hold. Notice that the momentum sum rule provides almost no constraint since the amount of momentum carried by gluons in the region $x < 0.01$ is small, whichever form is used there. Figure 5 compares the resulting gluon distributions at higher Q^2. The two starting forms are equal for $x > 0.02$ ($Q_0^2 = 5GeV^2$) and have the forms

of equations 17 and 19 at smaller x the first of these is the EHLQ set 2 (see below). I will refer to the other as EHLQ2′. Notice that the differences become less important at large Q^2. The uncertainties in predicted rates due to the small x problem are therefore serious only for processes sensitive to small x and Q^2.

3. Parameterizations of distribution functions.

I will now discuss briefly some of the more commonly used of parton distribution functions. There are many sets of distribution functions coming from fits to the data using lowest order QCD. The most frequently used of these are the two sets of Duke and Owens[5] (DO1 and DO2) which were based on data from EMC,[12] SLAC[9] and CDHS[16] (the latter were renormalized in an attempt to deal with the systematic differences in the data sets, see above), and Eichten *et al.*[23] (EHLQ1 and EHLQ2) based primarily on the CDHS data. These pairs correspond to different shapes for the gluon distribution and consequently different values of α_s (or Λ). As usual the gluon distribution with more support at large x (harder distribution) corresponds to the larger value of α_s (EHLQ2 and DO2). Parameterizations of these distribution functions are given in the papers and can easily be applied to a variety of other processes.

Recently, fits using next to leading order QCD have emerged. Diemoz, Ferroni, Longo and Martinelli (DFLM)[25] used neutrino data from BEBC,[18] CCFRR,[25] CHARM[14] and CDHS.[17] They also provide different fits corresponding to different values of α_s. They give sets of distribution functions corresponding to a range of Λ[‡] viz $\Lambda = 160,\ 260,\ 360$ MeV. These fits are used to estimate the uncertainties in top quark rates at the Tevatron and $Sp\bar{p}S$ colliders. The fits are only available in the form of a computer program from the authors.

Martin, Roberts and Stirling[27] (MRS) have used EMC[12] data together with that from CDHSW[17] and CCFRR[15] (to which they apply a renormalization of order 10%, see the discussion above following equation 16). They present

[‡]Here I am quoting a Λ which corresponds to 4 flavors, in the range $m_{charm} < Q < m_{bottom}$ the formula for α_s is $\alpha_s = \frac{12\pi}{25\log(Q^2/\Lambda^2)}[1 - \frac{462}{625}\frac{\log\log(Q^2/\Lambda^2}{\log(Q^2/\Lambda^2)}]$. See reference 20 for a summary of the behavior of this formula as a threshold is crossed.

three fits which differ in the form of $xg(x, Q^2 = 4GeV^2)$.

$$\begin{aligned} xg(x, Q^2 = 4GeV^2) &\sim (1-x)^5 && (set\ 1) \\ &\sim (1-x)^4(1+9x) && (set\ 2) \\ &\sim x^{-1/2}(1-x)^6(1+9x) && (set\ 3). \end{aligned} \tag{20}$$

They then use data from J/ψ production[28] and photon production[29] at large transverse momentum which is sensitive to the shape of the gluon distribution (see below) in an attempt to distinguish between the sets. They conclude that set 1 is slightly preferred. These fits are not available in a convenient parameterization, although a computer program to generate them is available from the authors.

Recently[30] they have refitted set 1 using the BCDMS[10] data instead of EMC.[12] Here they find that the neutrino data and BCDMS are compatible and that a renormalization of the former is not needed. They have compared the predictions from these two sets of distributions with the data on Drell–Yan production at the ISR.[31] The BCDMS fit is preferred, but the order α_s QCD corrections to the Drell–Yan rate are quite large and the α_s^2 terms are not known so any definite conclusion seems premature.§ DFLM and MRS do not use the same scheme to define distribution functions, hence their results are not strictly comparable; one must compute a physical quantity such as F_2 to facilitate a comparison. DFLM use a physical scheme so that the equation

$$F_2(x, Q^2) = 2x \sum_i e_i^2 q_i(x, Q^2) \tag{21}$$

is maintained beyond leading order. In the MRS scheme there are finite corrections to this relationship proportional to α_s. The gluon distributions are defined so that they satisfy the momentum sum rule. It may be better to define

§Recently Tung[32] has claimed that there may be a problem with the evolution program of MRS in the small x region. He claims that their evolution is generates a value for $xg(x, Q^2)$ which is too large for $x < 0.01$. A comparison of his evolution with that of DFLM shows perfect agreement.

the gluon distribution in terms of a physical process known to beyond leading order in α_s. Candidates include heavy quark[33] or jet production[34,35] in hadron–hadron production or photo–production.[36]

Since these next to leading order fits are only available in the form of a computer code, it is worth remarking that a package is available from Tung[37] that, given a set of input distribution functions, will generate distributions functions in leading, or next to leading, order.

In figures 6 and 7, I show a comparison of the various gluon distributions from the parameterizations discussed above. It can be seen that, as expected the differences are greatest at small Q^2. Subsequently I shall use these fits to give an indication of the errors in predicted rates. I do not believe that, given the systematic discrepancies between the data sets, it is possible to give truly meaningful errors (i.e. one standard deviation) on the predicted rates.

4. Use of Distribution Functions to Predict Cross–Sections.

Consider the parton model applied to the calculation of some process in a hadron–hadron collision. The hadronic cross–section σ is given in terms of the partonic cross section $\hat{\sigma}_{ij}$ by

$$\sigma \sim \sum_{ij} \int dx_1 dx_2 \hat{\sigma}_{ij} f_i(x_1, M^2) f_j(x_2, M^2). \tag{22}$$

Here the sum runs over all types of partons that contribute to the process and the f_i are the parton distribution functions. The parton cross section σ_{ij} can be expressed as an expansion in $\alpha_s(\mu)$

$$\hat{\sigma}_{ij} = A\alpha_s^n(\mu)(1 + B\alpha_s(\mu)\ldots). \tag{23}$$

Before expression (22) can be used we must (a) calculate $\hat{\sigma}$, (b) have a set of distribution functions and (c), choose the scales M and μ. (a) is straightforward although it can be extremely tedious. (b) has been discussed above. Recall the discussion of the definition of q_i (see equation 14 and the surrounding discussion), and that the form of $\hat{\sigma}$ will depend upon this definition. From equation 13, it is clear that a change in the scale M to M' will induce a term in equation 22

of order $\alpha_s \log(M'/M)$. An intelligent discussion of the scale dependence is not possible therefore unless $\hat{\sigma}$ is known to beyond leading order in α_s since a shift in scale is equivalent to a higher order correction. The uncertainties due to the choice of scale would vanish completely if the calculation could be done to all orders in α_s. In this case a shift in M would merely change the separate terms in the expansion; the full result would not change. In practice (23) is know only to leading or next to leading order so that M or μ dependence remains. I shall set $M = \mu$ in the following although there is no necessity to do so.

It is clear that M should be of the order of the momentum transfers in the partonic process. Large higher order corrections are likely to result from an unphysical choice. If the next to leading order corrections are known, the M dependence can be investigated with a view to "picking the right M". There are two popular ways of choosing M; fastest apparent convergence (FAC) and minimal sensitivity (PMS).[38] In the former, one chooses the M which makes the next to leading order term small; in the latter, the M where the total result is varying least with M. The motivation in the latter case being that the result to all orders is independent of M. In my view neither of these choices should be used if they give rise to unphysical scales.

It is possible that the uncertainty due to the choice of M could be greater than that due to poor knowledge of the distribution functions. If this is the case then the process cannot make a useful contribution to distribution function determinations. I will now use some examples to illustrate the issues discussed above and will begin with production of photons in pp and $p\bar{p}$ collisions.

At lowest order in α_s the processes $q\bar{q} \to \gamma g$ and $gq \to g\gamma$ contribute to photon production at large transverse momentum ($p_\perp$) in hadron–hadron collisions.[29,39] The former process is irrelevant in the accessible $p_\perp$ range at the Tevatron collider so the photon production offers a direct probe of the gluon distribution. At next order in α_s the processes such at $gg \to q\bar{q}\gamma$ can contribute. This contribution is large if the photon is collinear with an outgoing quark. Fortunately this configuration is difficult to observe experimentally since the

photon is buried inside a jet; therefore a cut requiring that the photon be isolated is usually applied.

Figure 8 shows the predicted $p_\perp$ spectrum for the production of photons at the Tevatron collider. Two bands are shown corresponding to the predicted rates in leading order and next to leading order QCD[40] when the scale $M = \mu$ is varied from $p_\perp/2$ to $2p_\perp$. The result from the next to leading order where M is chosen according to the PMS scheme is also shown. It is larger since the scheme picks $M \sim p_\perp/3$, a value that is, perhaps, too small. Figure 9 shows the ratio of the value at the top of the bands in figure 8 to that at the bottom. The figure clearly shows that the uncertainty is reduced when the higher order corrections are included. I have also indicated on this figure the width of a band in predictions caused by varying the distribution functions. It is clear that given the uncertainties associated with the choice of scale the sensitivity to different distribution functions is limited. However, analyses comparing to data from the ISR[29] and UA2[39] conclude that a softer gluon distribution such as MRS1, DO1 or EHLQ1 is preferred.[27] More information can possibly be obtained by looking at the rapidity distribution of the photons. Figure 10 shows such a prediction for the EHLQ2 and EHLQ2′ distribution functions. The peak at large y in the latter case is due to the more singular form of $xg(x, Q^2)$ at small x.

Measurements of the photon production at FNAL fixed target energies[41] are complimentary to those at the collider since a different range of x is explored. Figure 11 shows the $p_\perp$ distribution for a few representative sets of structure functions. For the values of $p_\perp$ shown here the uncertainty due to the scale choice M (varied from $p_\perp/2$ to $2p_\perp$) is about a factor of 3.

The production of photon pairs at the Tevatron can also be a probe of the gluon distribution since, at the accessible values of $p_\perp$ the process $gg \to \gamma\gamma$ is dominant over $q\bar{q} \to \gamma\gamma$.[42] The next order QCD corrections to this process are not known, hence the M dependence is rather large. Figure 12 shows the predicted rate for a representative set of distribution functions.

I would now like to discuss another process for which the next to leading

order QCD corrections are known: the production of a top quark pair at the Tevatron collider. At lowest order in QCD, there are two relevant processes, $gg \rightarrow t\bar{t}$ and $q\bar{q} \rightarrow t\bar{t}$. Figure 13 shows the production cross-section for a top quark pair as a function of the scale M. The DFLM[25] ($\Lambda = 260MeV$) distribution functions are used. When the next to leading order calculation is used there is an uncertainty of order $\pm 10\%$ from this scale ambiguity if we vary M from $m_{top}/2$ to $2m_{top}$.[34] Notice that the FAC (where the higher order corrections is zero) and PMS (the stationary point on the solid curve) choices are similar and correspond to $M \sim m_{top}/3$. Table 1 shows the spread in predicted cross-sections from the different sets of distribution functions. This spread is larger than $\pm 10\%$, hence the primary uncertainty in top production rates, and therefore on a limit on the top quark mass if no events are seen, is due to distribution functions. Even so it is fair to conclude that we understand these rates to better than a factor of two.

The situation with regard to bottom quark production at the Tevatron is not so clear. Firstly the M dependence of the cross-section is quite large and indeed is stronger if the next to leading order terms are included.[34] An uncertainty of $\pm 30\%$ due to M exists. In addition the values of x (of order $m_{bottom}/\sqrt{s}$) and relatively low Q^2 are in a region where the uncertainties due to the low x behavior of the distribution functions are large. Figure 14 shows the total $b\bar{b}$ production rate in pp collisions as a function of $\sqrt{s}$ with $M = m_{bottom}$; the two curves correspond to EHLQ2 and EHLQ2′ distributions. One can see from this that the uncertainties get worse as $\sqrt{s}$ rises. An uncertainty of at least a factor of 4 exists in the rates predicted at the SSC. In order to reduce this, we need information on the gluons at small x since the $gg \rightarrow b\bar{b}$ process is dominant.

Next to leading order corrections to the $2 \rightarrow 2$ parton scattering processes which give rise to two jet production in hadron-hadron collisions have been calculated,[34] but they have not yet been implemented in a calculation of the inclusive jet cross-section. Figure 15 shows the jet rate using the EHLQ2 distri-

bution functions with the choices $M = p_\perp/2$ and $M = 2p_\perp$. By contrast, figure 16 shows the same rate for a selection of distribution functions with $M = p_\perp$. A comparison of these figures reveals that the uncertainties due to the distribution functions is not the limiting factor at present. As in the case of photon production a quantity more sensitive to the distribution functions is the jet's rapidity distribution since at large rapidity it is sensitive to smaller values of x for a given $p_\perp$. The biggest differences arise at small $p_\perp$ where it may be more difficult to get good data.

There are some other processes which may be a good probe of distribution functions. The production of muon pairs of large invariant mass (Drell–Yan process) proceeds via quark anti–quark annihilation and can provide an indirect constraint on the gluon distribution since antiquarks in the proton are produced from the gluons by the Q^2 evolution of distribution functions. The rapidity distribution of the Drell–Yan pairs at the Tevatron[43] may afford a probe of the gluons at small x where effects similar to those indicated for photon production (see figure 10) may occur. W/Z production at the $Sp\bar{p}S$ and Tevatron colliders provide a probe of the antiquark distributions, but the relevant values of x are quite large (.13 and .04) for W/Z's produced centrally and at these values the quark (antiquark) distribution in a proton (antiproton) is well known.

The production of J/ψ in proton–proton collisions[28] has been advocated[27] as a probe of the gluon distributions since theoretical models [44] for the production include the processes $q\bar{q} \to J/\psi$ and $gg \to J/\psi$. In the latter case one or more gluons must be emitted in order to conserve color. Absolute predictions for the rate are model dependent and unreliable. Nevertheless, if one assumes that the rate has two components

$$\sigma \sim g(x, Q^2)g(x_2, Q^2)\sigma_1 + q_i(x_1 Q^2)\bar{q}_i(x_2, Q^2)\sigma_2 \qquad (24)$$

it is possible by studying the rapidity dependence of the production rate to get some information on the shape of the gluon distribution ($y_\psi = 0.5 \log(x_1/x_2)$). Here an assumption is made that there is not additional rapidity dependence in σ_1. One is really assuming that the extra emitted gluons are all soft. MRS have

used the this to infer that the softer gluon distribution of their set 1 is preferred. The model for J/ψ production at large p_t is in better shape theoretically; here the dominant process is $gg \rightarrow gJ/\psi$ which can be calculated.[45]

Data from photoproduction either using a photon beam or in an ep or μp collision where the photon is only slightly off shell can also yield useful information on the gluon distribution. Heavy flavors are produced by the process $\gamma g \rightarrow Q\overline{Q}$. Next to leading order QCD corrections are known.[36] In the case of charm production, they are large and the process is probably not useful for a detailed test or determination of the gluon distribution. Bottom production either at FNAL[46] or HERA should provide useful information.

I will conclude this brief survey with some comments concerning HERA. The accessible range of x and Q^2 is vastly larger than that currently accessible. This will have two important consequences for the determination of structure functions. First, data will be available at values of x that are currently too small to be probed and some of the uncertainties (for example in the predicted bottom production rate at the SSC) should be considerably reduced. Second it may be possible to determine the gluon distribution directly by measuring

$$F_L = F_2 - 2xF_1 = \frac{\alpha_s}{2\pi}\int_x^1 \frac{dy}{y^3}\left[F_2(y) + (1 - x/y)\, yg(y)\right]. \qquad (25)$$

This is shown in figure 17. At values of x less than 0.05 the gluon term is dominant so that a measurement of F_L is a direct probe of the gluon distribution. A study of the feasibility of this measurement at HERA indicates that it may be possible to distinguish between current sets of gluon distributions.[46] Recall that the differences are greatest at small Q^2, but F_L will be dominated by incalculable higher twist $(1/Q^2)$ terms if Q^2 is too small. On figure 17, I have indicated the size of error that a HERA experiment can expect to reach.[47] It is clear that distinguishing between currently acceptable gluon distributions will not be easy but that it should be possible to discriminate between the different small x extrapolations.

In order to determine all of the parton distributions at HERA, and possibly also to determine Λ with an error smaller than the current one, it will be nec-

essary to measure the charged and neutral current scattering of both electrons and positrons off both protons and deuterons.

4. Conclusions

If one is interested in using QCD to calculate background rates at, for example, the Tevatron or $Sp\bar{p}S$ collider, then the uncertainties associated with the poor knowledge of parton distribution functions is less than a factor of 2 for almost all processes. Exceptions are processes that involve small total energy in the partonic system and hence very small values of x and Q^2. If one is interested in making a test of the standard model or in better determining distribution functions other factors such as the intrinsic uncertainty in parton model calculations due to choice of scale can be the limiting factors. All recent fits to data indicate that a softer gluon distribution of the form $xg(x,5) \sim (1-x)^5$ is a reasonable fit. There is considerable uncertainty about the behavior the distributions at small x, although this probably has few critical consequences elsewhere. Data from CDF on photon and Drell–Yan rates should help to resolve these uncertainties. The next qualitative improvement is not likely to occur until data from HERA become available.

References

1. For a review of the QCD parton a model see G. Altarelli *Phys. Rev.* **81C**, 1 (1982).

2. V. Papavassiliou (EMC collaboration) Proc. of Int. Europhysics Conference on High Energy Physics, Uppsala (1987).

3. A. Mueller, these proceedings.

4. For a review of the data and possible theoretical implications see F.E. Close Tennessee preprint (1988); V. Barone and E. Predazzi, Annals de Physique (to appear), or E. Berger in Proc of 23rd International Conf. on High Energy Physics, Ed. S. Loken, World Scientific Publishing (1987).

5. R. Brinkman "HERA" DESY-HERA-88-03 (1988).

6. G. Altarelli and G. Parisi, *Nucl. Phys.* **B126**, 298 (1977).

7. For a review see A. H. Mueller in Proc. 1985 TASI Summer School, Ed. F. Gersey, World Scientific Publishing (1986).

8. See also F.J. Sculli, Talk at 1988 Arles Conference, June 1988, and R. Voss in Proc. of 1987 International Symposium on Lepton and Photon Interactions at High Energies, Hamburg 1987.

9. A. Bodek *et al.*, *Phys. Rev.* **D20**, 1471 (1979).

10. A. Benvenuti *et al.*, *Phys. Lett.* **195B**, 91 (1987).

11. A. Benvenuti *et al.*, JINR–E1–87–689, 699 (1987).

12. J.T. Aubert *et al.*, *Nucl. Phys.* **B293**, 740 (1987); **B272**, 158 (1986), **B259**, 189 (1985); or M. Arneodo *et al.*, *Nucl. Phys.* **B264**, 739 (1986).

13. P.D. Meyers, *et al.*, *Phys. Rev.* **D34**, 1265 (1986).

14. J.V. Allaby, *et al.*, *Phys. Lett.* **197B**, 281 (1987), CERN EP/87/225. F. Bergsma *et al.*, *Phys. Lett.* **123B**, 269 (1983), **153B**, 111 (1985).

15. D. B. Macfarlane et al., *Zeit. fur Physik* **C26**, 1 (1984).

16. H. Abramowicz, *et al.*, *Zeit. fur Physik* **C17**, 283 (1983).

17. H. Abramowicz, *et al.*, *Zeit. fur Physik* **C35**, 443 (1987); B. Vallage, Thesis submitted to Université de Paris Sud (1984).

18. D. Allasia *et al.*, *Phys. Lett.* **135B**, 231 (1986); *Zeit. fur Physik* **C28**, 321 (1985).

19. F.J. Sculli Ref. 8.

20. R.M. Barnett, I. Hinchliffe and J. Stirling in Review of Particle Properties *Phys. Lett.* **204B**, 1 (1988).

21. J. Morfin, private communication.

22. J. Collins in "Supercollider Physics" Ed. D. Soper, World Scientific publishing (1987).

23. E. Eichten *et al.*, *Rev. Mod. Phys.* **56**, 579 (1984).

24. D. Duke and J. Owens *Phys. Rev.* **D30**, 49 (1984).

25. M. Diemoz, F. Ferroni, E. Longo, and G. Martinelli, CERN–TH–4757 (1987).

26. G. Altarelli, *et al.*, CERN–TH–4978 (1988).

27. A.D. Martin, R.A. Roberts and J. Stirling, *Phys. Rev.* **D37**, 1161 (1988).

28. J.A. Branson *et al.*, *Phys. Rev. Lett.* **38**, 1331 (1977); K.J. Anderson *et al.*, *Phys. Rev. Lett.* **42**, 944 (1979); E.J. Siskind *et al.*, *Phys. Rev.* **D21**, 628 (1980).

29. T. Akesson, *et al.*, *Zeit. fur Physik* **C34**, 293 (1987).

30. A.D. Martin, R.G. Roberts and J. Stirling, *Phys. Lett.* **207B**, 205 (1988).

31. D. Antreasyan *et al.*, *Phys. Rev. Lett.* **48**, 302 (1982).

32. W-K. Tung, private communication and talk at 1988 DPF Summer Study on High Energy Physics in the 1990's, Snowmass, Colorado, July 1988.

33. S. Dawson, R. K. Ellis and P. Nason, *Nucl. Phys.* **B303**, 607 (1988).

34. R.K. Ellis and J.C. Sexton, *Nucl. Phys.* **B269**, 445 (1986).

35. P. Chiapetta, Talk at 1988 Workshop on $p\bar{p}$ physics, FNAL,

36. R. K. Ellis and P. Nason, FNAL 88/54–T (1988).

37. W-K. Tung, Int. J. Mod Phys. **A2**, 1369 (1987).

38. P.M. Stevenson, *Nucl. Phys.* **B231**, 65 (1984).

39. J.A. Appel *et al.*, *Phys. Lett.* **176B**, 239 (1986).

40. P. Aurenche, R. Baier, A. Douiri and D. Schiff, *Phys. Lett.* **169B**, 441 (1986), *Phys. Lett.* **140B**, 87 (1984).

41. F. Lokowicz *et al.*, in "Elementary Hadronic Processes and Heavy Ion Interactions" Ed. Tran Truong (1982).

42. B.L. Combridge, *Nucl. Phys.* **B174**, 243 (1980).

43. F. Olness and W-K. Tung, Int. J. Mod. Phys. **A2**, 1413 (1987).

44. M. Gluck, J. Owens and E. Reya, *Phys. Rev.* **D17**, 2324 (1978).

45. R. Baier and R. Ruckl, *Phys. Lett.* **102B**, 364 (1981).

46. J.A. Appel, FNAL-CONF-88/22 (1988).

47. A.M. Cooper-Sarkar, *et al.*, RA 87–112.

Figure Captions

Figure 1: Diagram illustrating the kinematics of deep inelastic scattering.

Figure 2: A comparison of $F_2(x, Q^2)$ measured in muon scattering from a proton target from the BCDMS[1] (closed dots) and EMC[12] collaborations (open circles). Also shown are data at small Q^2 (boxes) from the electron scattering experiment[9] at SLAC.

Figure 3: The ratio R_1 (equation 16) plotted against x the data are from EMC[12] ($F_2^{\mu N}$) and CCFRR[15] ($F_2^{\nu N}$) both of which use an iron target. Figure from Sculli, ref. 8.

Figure 4: The value of Λ_{QCD} as a function of the Q^2 mix cut applied to the BCDMS,[10] EMC[12] and BPF[13] data. The squares correspond to a lowest order QCD fit and the circles to next to leading order ($\overline{MS}$ scheme, 4 flavors). Figure courtesy J. Morfin.[21]

Figure 5: A comparison of the gluon distributions for fixed Q^2 as a function of x. The solid lines are EHLQ set 2 and the dashed are EHLQ2′ (see text). The higher (lower) curve at small x corresponds to $Q^2 = 50(5)$ GeV^2.

Figure 6: A comparison of the gluon distributions from various parameterizations at $Q^2 = 5$ GeV^2. Parametrizations shown are EHLQ1, EHLQ2, DO1, DO2, DFLM (Λ=160,260,360 MeV) and MRS1 (based on EMC and BCDMS).

Figure 7: As figure 6 except $Q^2 = 50$ GeV^2.

Figure 8: The cross section $d\sigma/dp_t dy$ for the production of a photon at $y = 0$ in $p\bar{p}$ collisions at $\sqrt{s} = 1.8$ TeV. The region between the dashed (solid) lines corresponds to the lowest order (next to lowest order) rates when $M = \mu$ is varied from $p_t/2$ to $2p_t$. The dashed line is the result of using the PMS scheme.

Figure 9: The ratio of the upper and lower ranges of the predictions shown in figure 8. The dashed (solid) line corresponds to leading (next to leading) order. Also shown (dotted line) is the ratio of the upper to lower range corresponding to changes in the structure functions. The upper range is given by DO2 and by MRS1 (EMC data), the lower by EHLQ2 ($\mu = M = p_t$ is used).

Figure 10: $\int_5^{15} \frac{d\sigma}{dp_\perp dy} dp_\perp$ as a function of y for the production of a photon in $p\bar{p}$ collisions at $\sqrt{s} = 1.8$ TeV. The solid (dashed) lines correspond to the EHLQ2 (EHLQ2′) distribution functions. Lowest order QCD with $\mu = M = p_t$ is used.

Figure 11: The cross section $d\sigma/dp_\perp dy$ at $y = 0$ for the production of a photon in pp collisions at $\sqrt{s} = 34$ GeV. The lines correspond to EHLQ2 (solid), DO2 (dashed), and DFLM (dotted) ($\Lambda = 260$ MeV) sets of distribution functions.

Figure 12: $d\sigma/dM_{\gamma\gamma}$ for the process $p\bar{p} \to \gamma\gamma + X$ at $\sqrt{s} = 1.8$ TeV. Here $M_{\gamma\gamma}$ is the invariant mass of the photon pair. Both photons are required to satisfy $|y| < 2.5$. The dashed (solid) line corresponds to the $EHLQ2'$ ($EHLQ2$) structure functions.

Figure 13: The dependence of the $t\bar{t}$ production rate upon $\mu = M$ for $m_{top} =$ 60 GeV at $\sqrt{s} = 1.8$ TeV in $p\bar{p}$ collisions in leading (dotted line) and next to leading order (solid line) using the DFLM ($\Lambda = 260$ MeV) distrinutionm functions.

Figure 14: The production rate for $b\bar{b}$ pairs in pp collisions as a function of $\sqrt{s}$. The distribution functions of EHLQ2 (solid line) and EHLQ2′ of (dashed line) are used.

Figure 15: The cross section $d\sigma/dp_\perp dy$ for the production of a jet at $y = 0$ in $p\bar{p}$ collisions at $\sqrt{s} = 1.8$ TeV. The curves correspond to the EHLQ2 set

distribution functions with $\mu = M = p_t/2$ (upper curve) and $\mu = M = 2p_t$ (lower curve).

Figure 16: The cross section $d\sigma/dp_\perp dy$ for the production of a jet at $y = 0$ in $p\bar{p}$ collisions at $\sqrt{s} = 1.8$ TeV. The lines correspond to DO2 (dashed), EHLQ2 (solid) and DFLM ($\Lambda = 260$, MeV, dotted) sets of distribution functions.

Figure 17: The structure function $F_L(x, Q^2)$ at fixed Q^2. The solid (dashed) lines correspond to $Q^2 = 50$ (5) GeV^2. The upper (lower) line at small x corresponds to the $EHLQ2'$ ($EHLQ2$) structure functions. The error bar indicates the size of error that can be expected[47] at HERA at $Q^2 = 50$ GeV^2

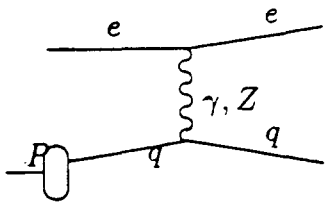

Figure 1

Figure 2

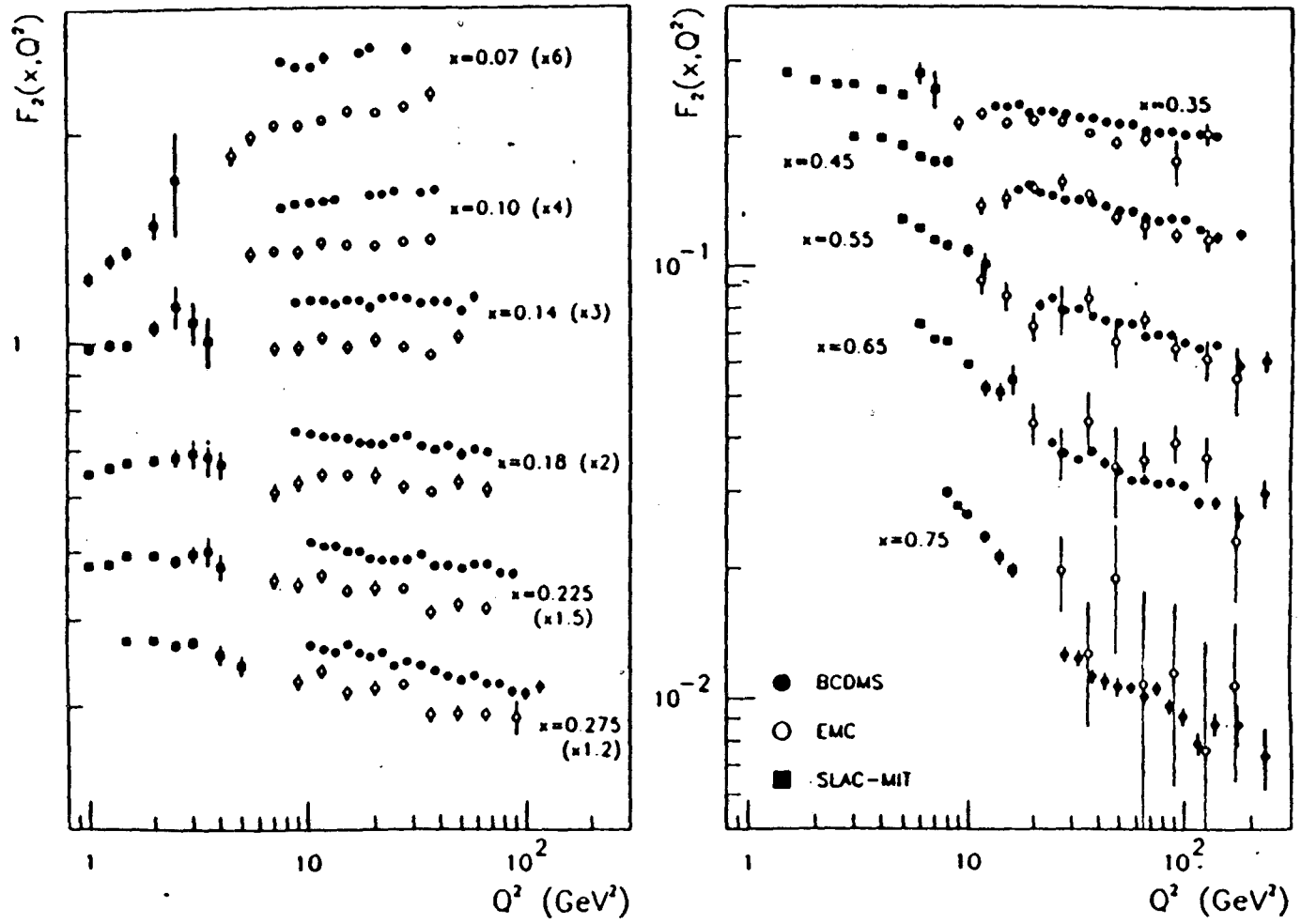
$F_2(x,Q^2)$
x=0.07 (x6)
x=0.10 (x4)
x=0.14 (x3)
x=0.18 (x2)
x=0.225 (x1.5)
x=0.275 (x1.2)
1
10
10^2
Q^2 (GeV^2)
$F_2(x,Q^2)$
x=0.35
x=0.45
x=0.55
x=0.65
x=0.75
10^{-1}
10^{-2}
BCDMS
EMC
SLAC-MIT
1
10
10^2
Q^2 (GeV^2)

Figure 3

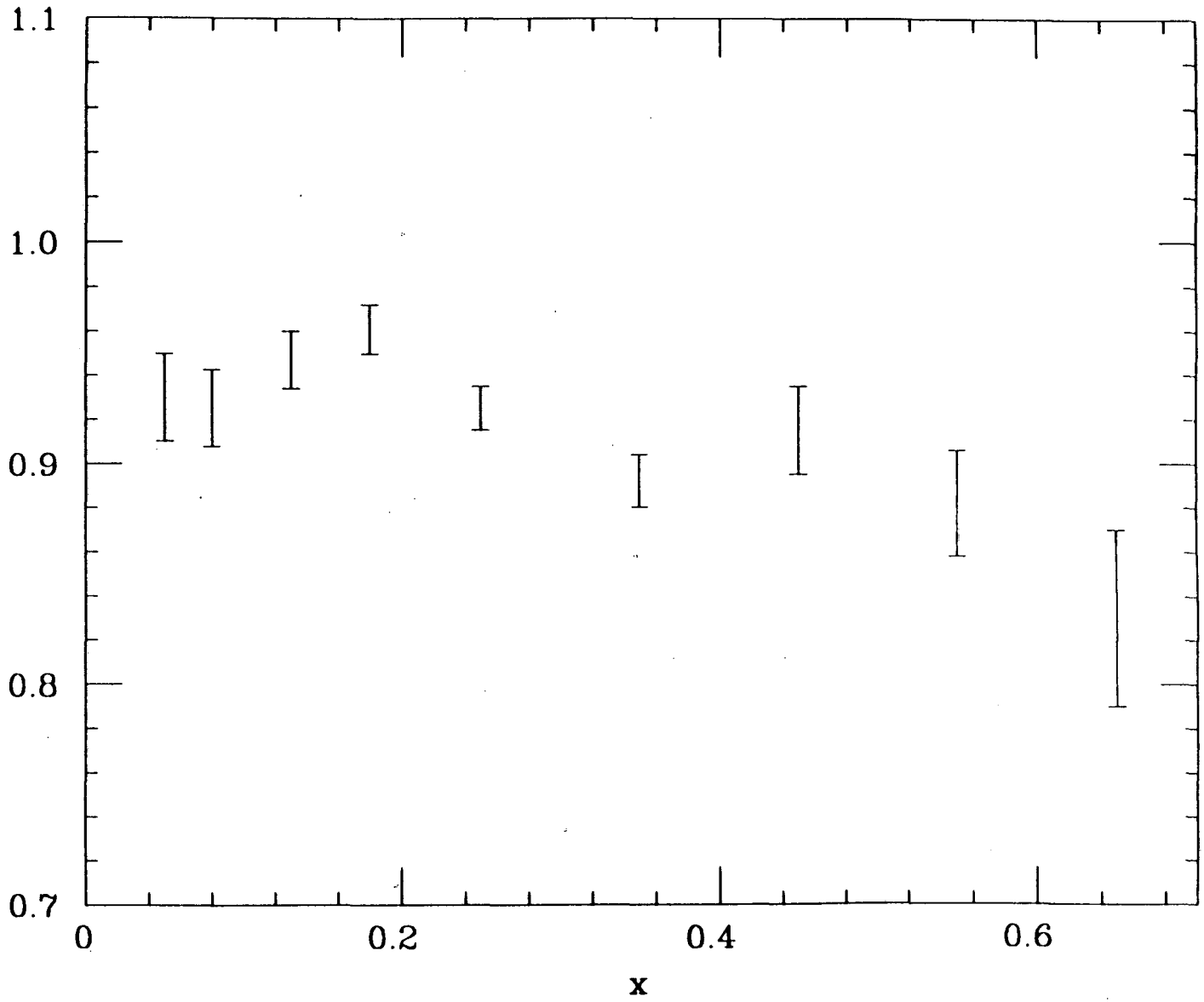

Figure 4

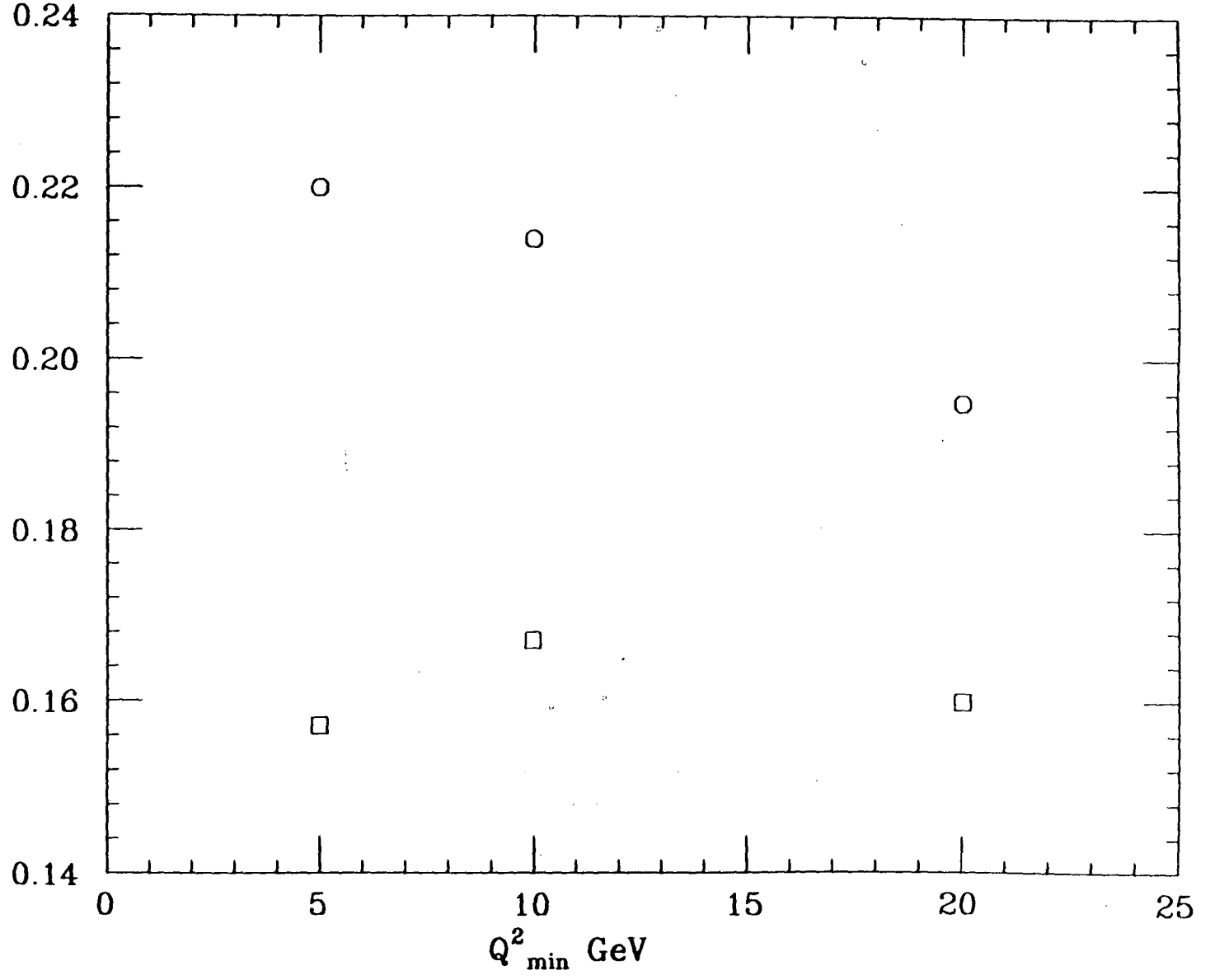

Figure 5

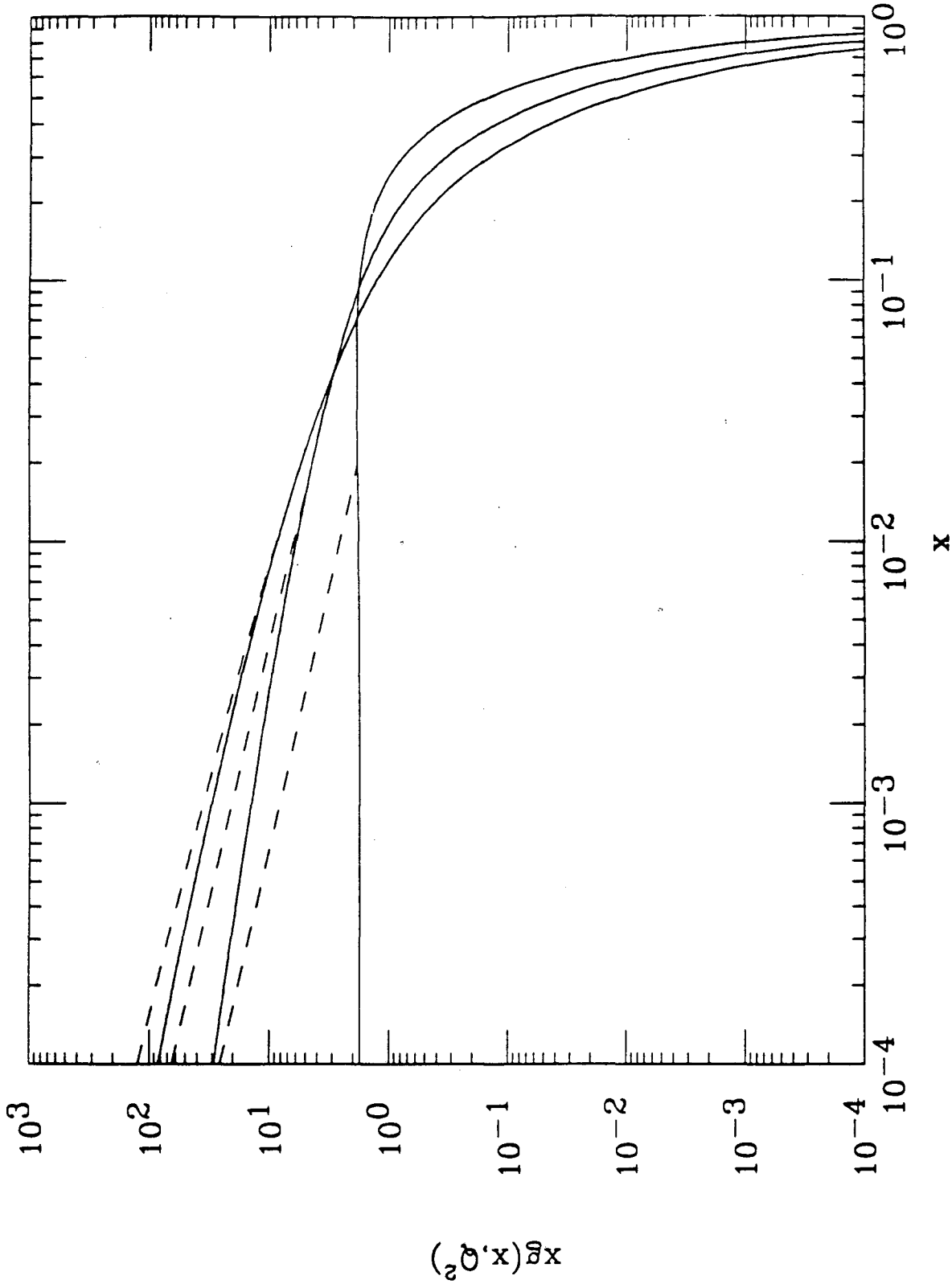

Figure 6

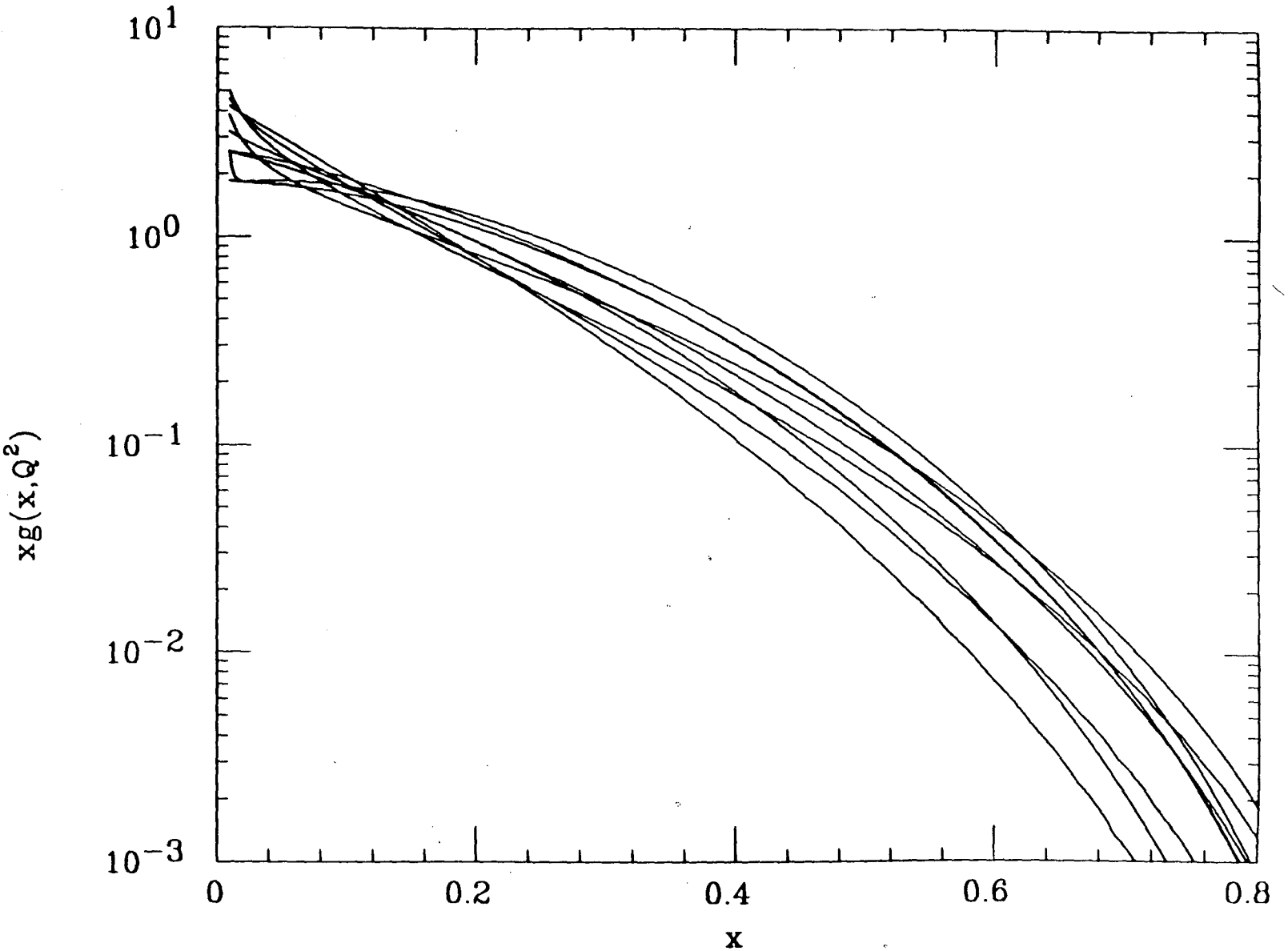

Figure 7

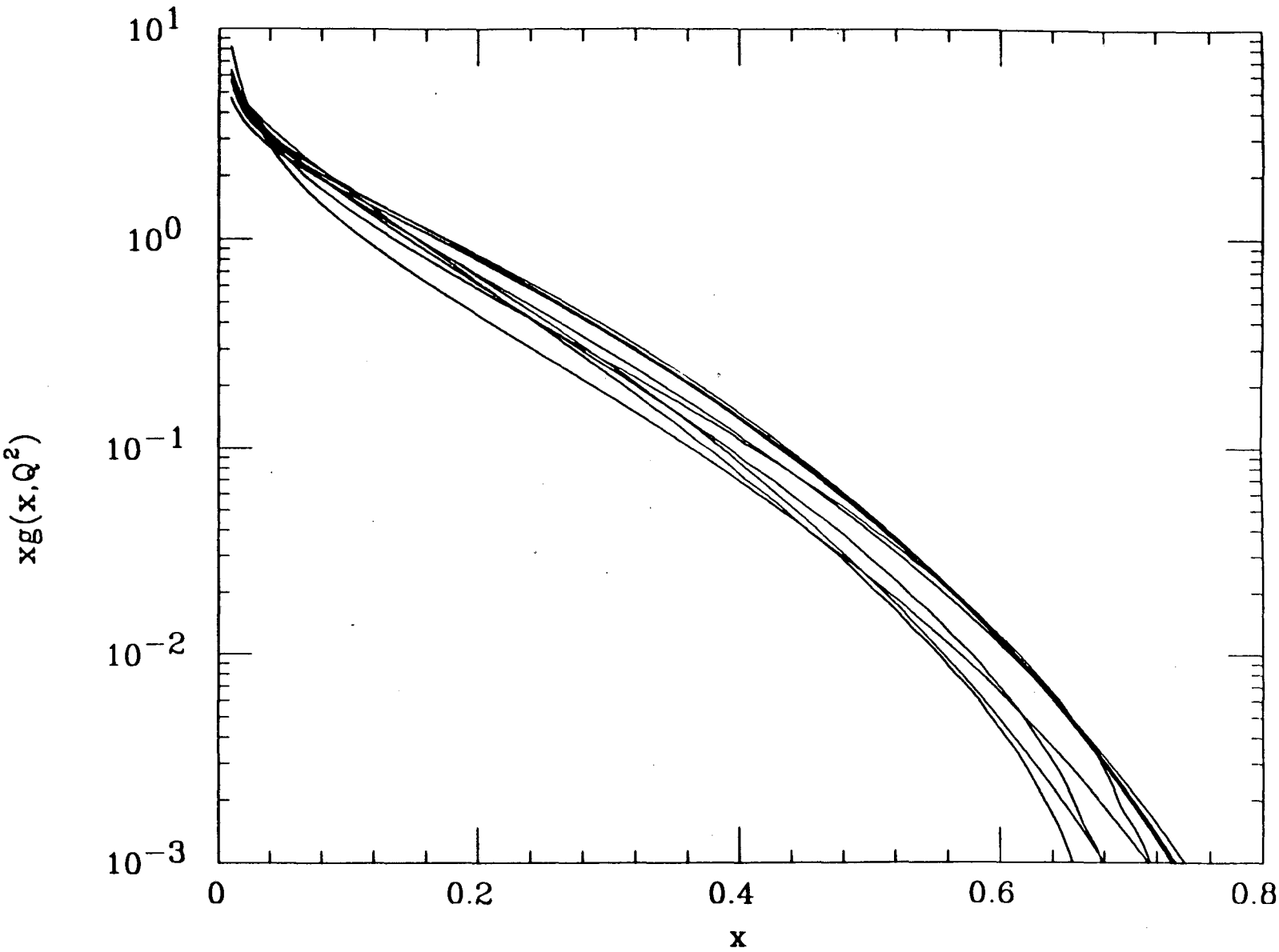

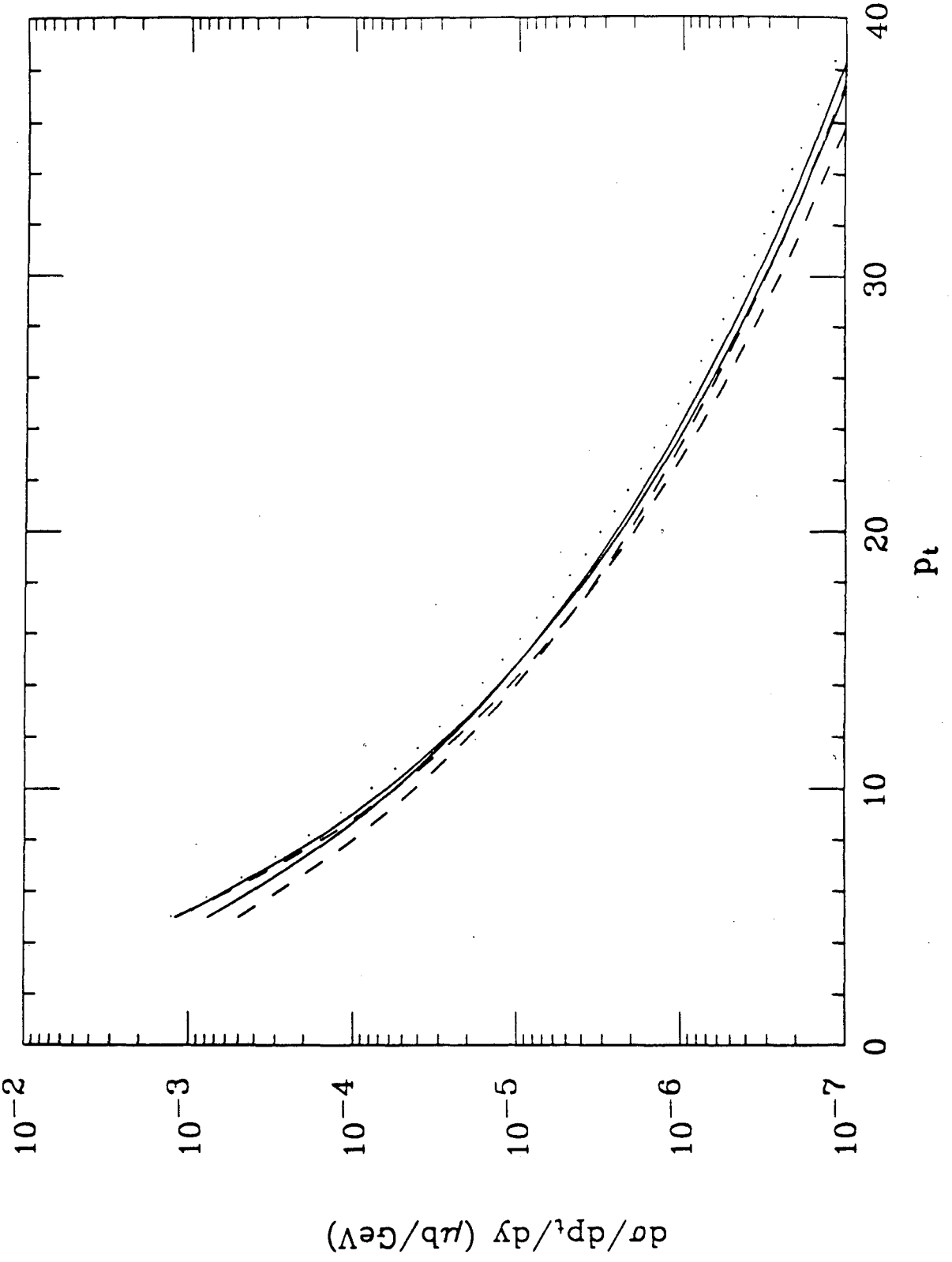

Figure 8

Figure 9

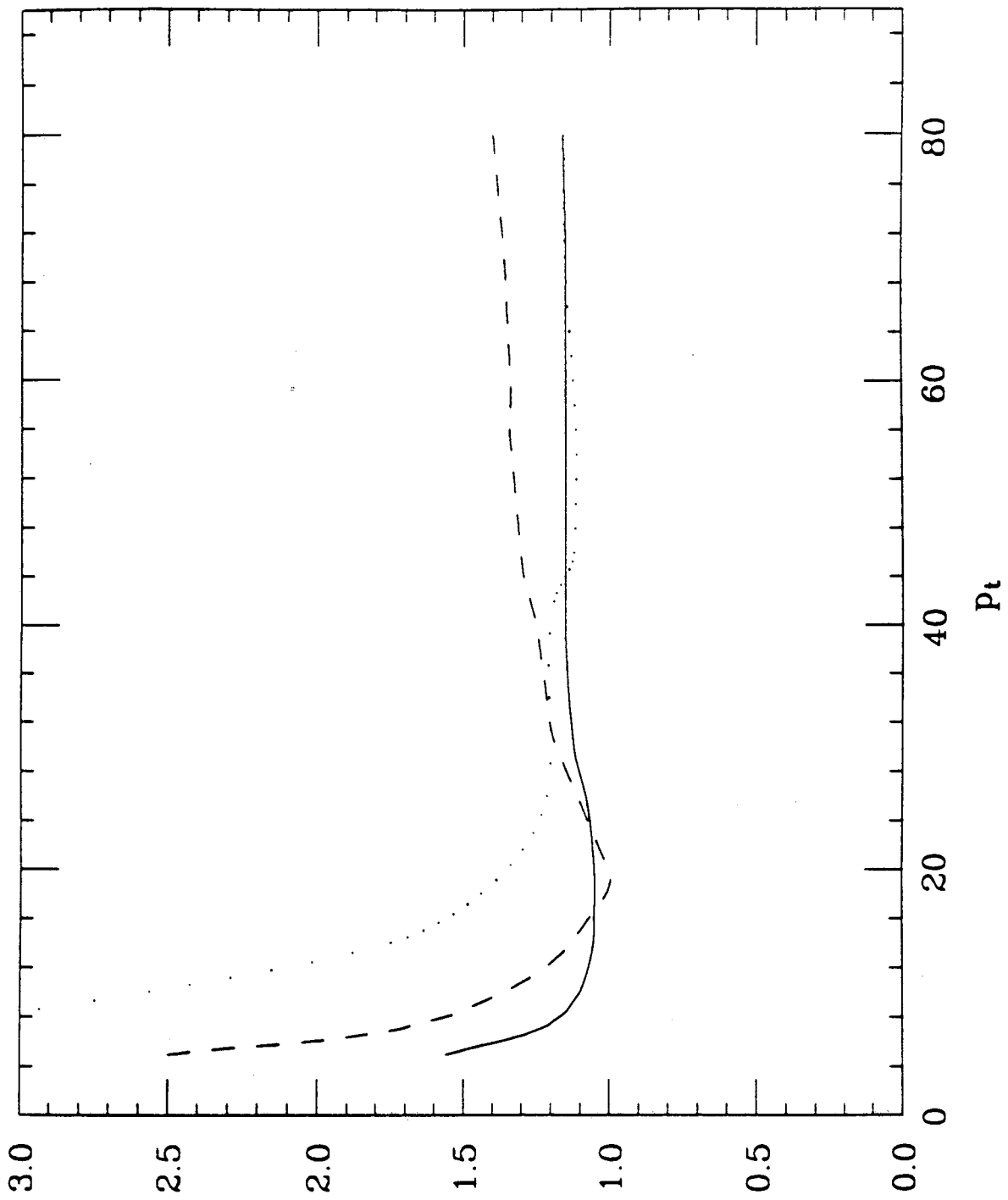

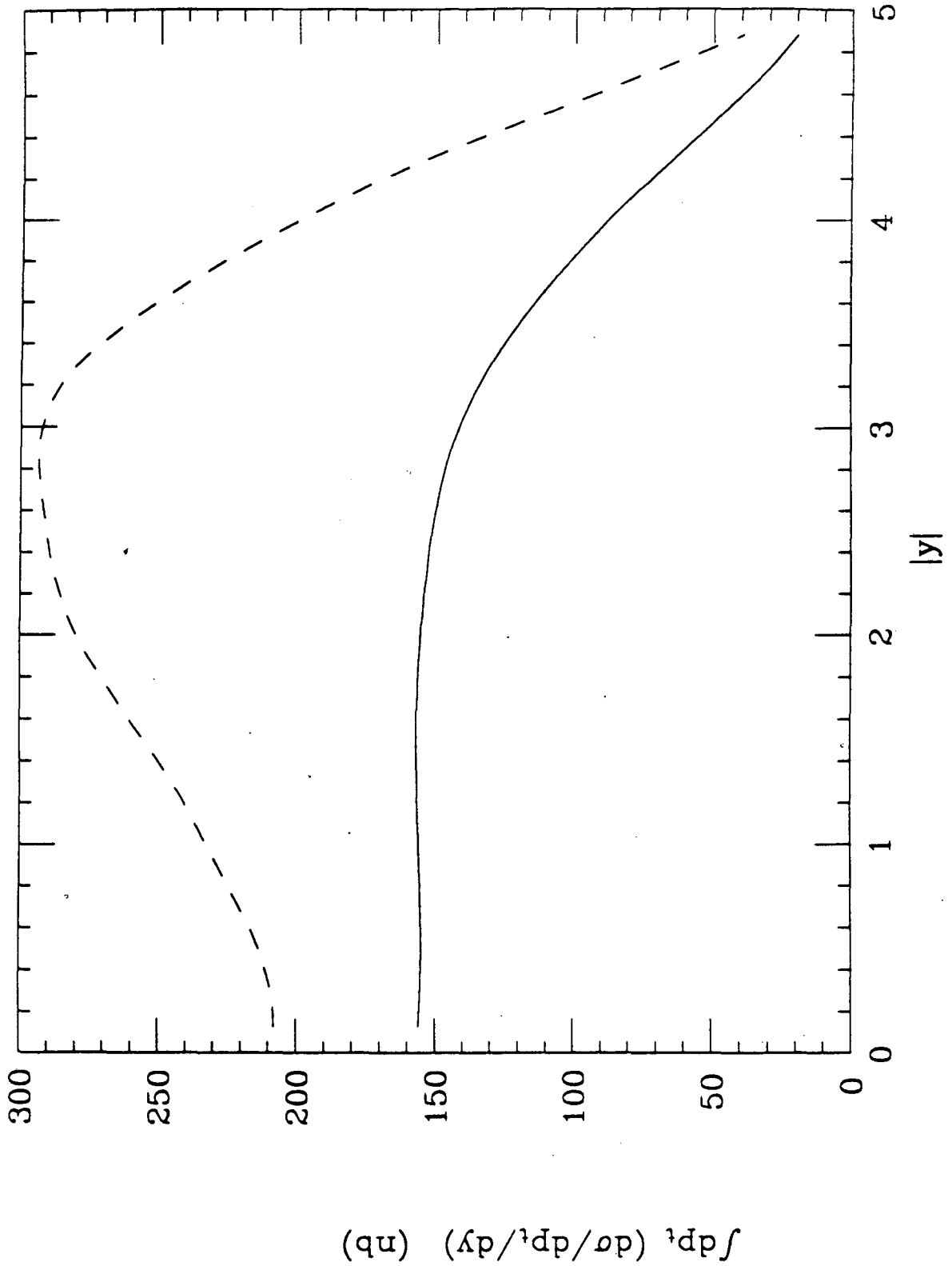
Figure 10
$\int dp_t\ (d\sigma/dp_t/dy)$ (nb)
|y|
0
50
100
150
200
250
300
0
1
2
3
4
5

Figure 11

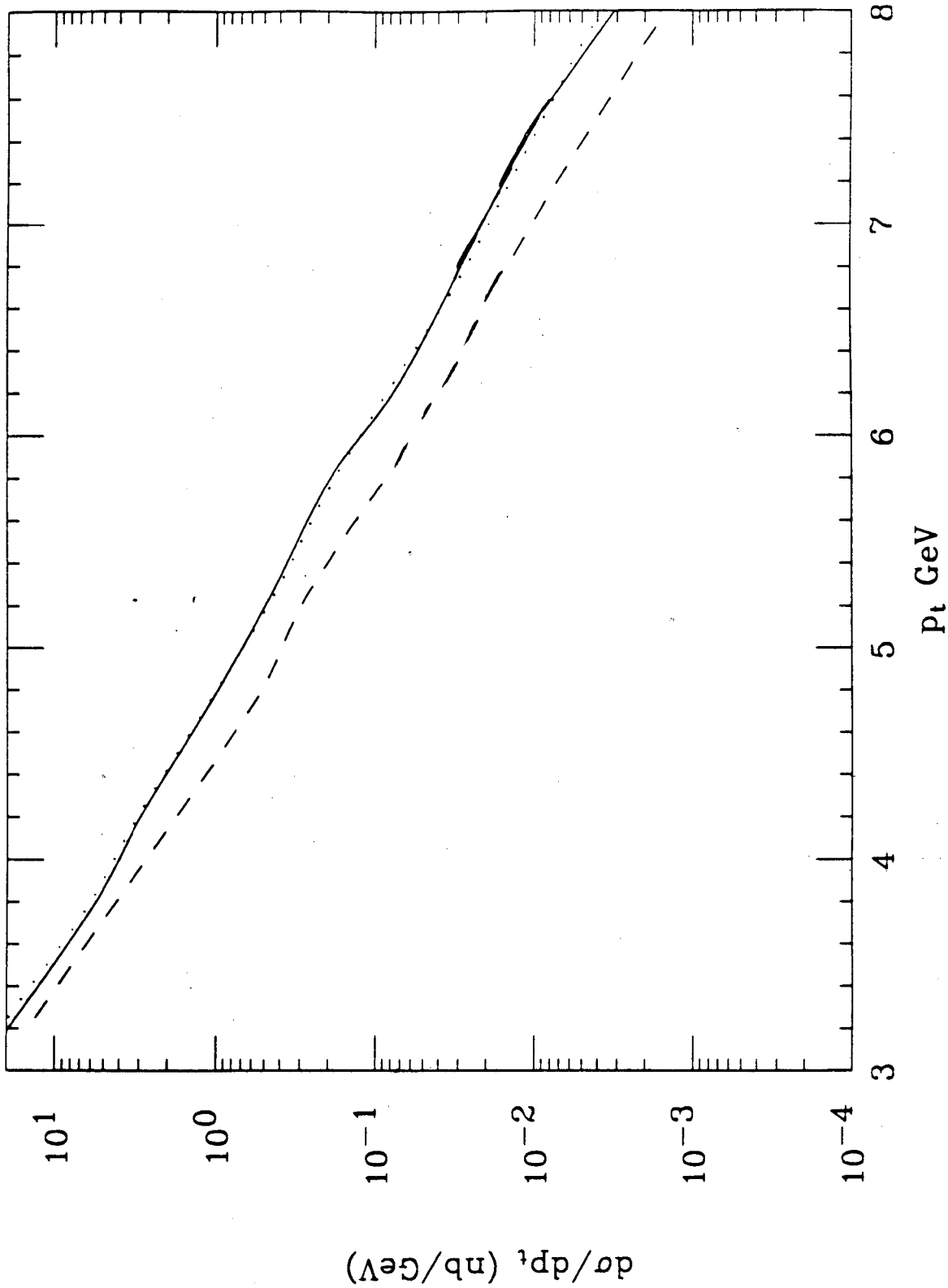

Figure 12

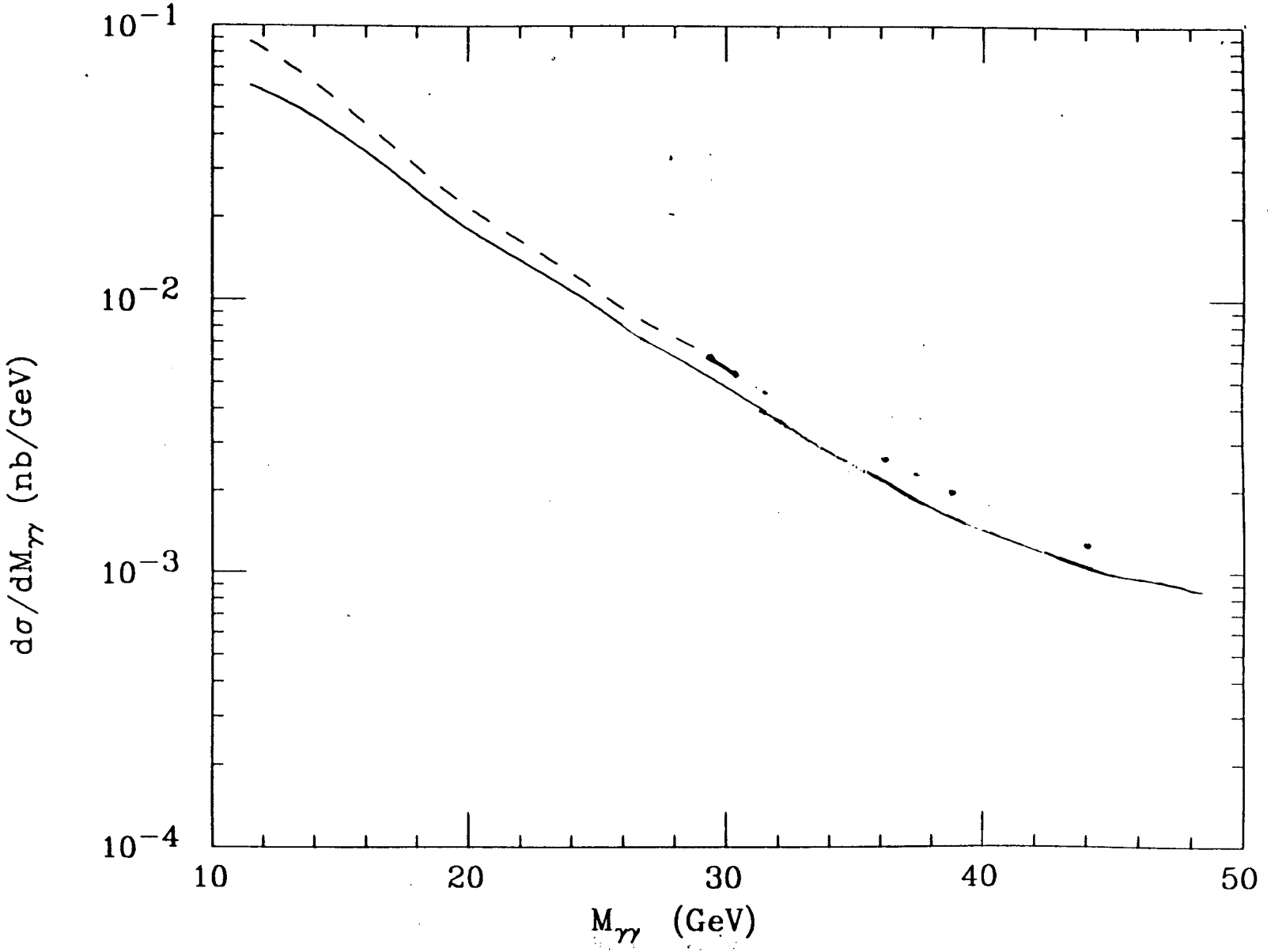
10^{-1}
10^{-2}
10^{-3}
10^{-4}
$d\sigma/dM_{\gamma\gamma}$ (nb/GeV)
10
20
30
40
50
$M_{\gamma\gamma}$ (GeV)

Figure 13

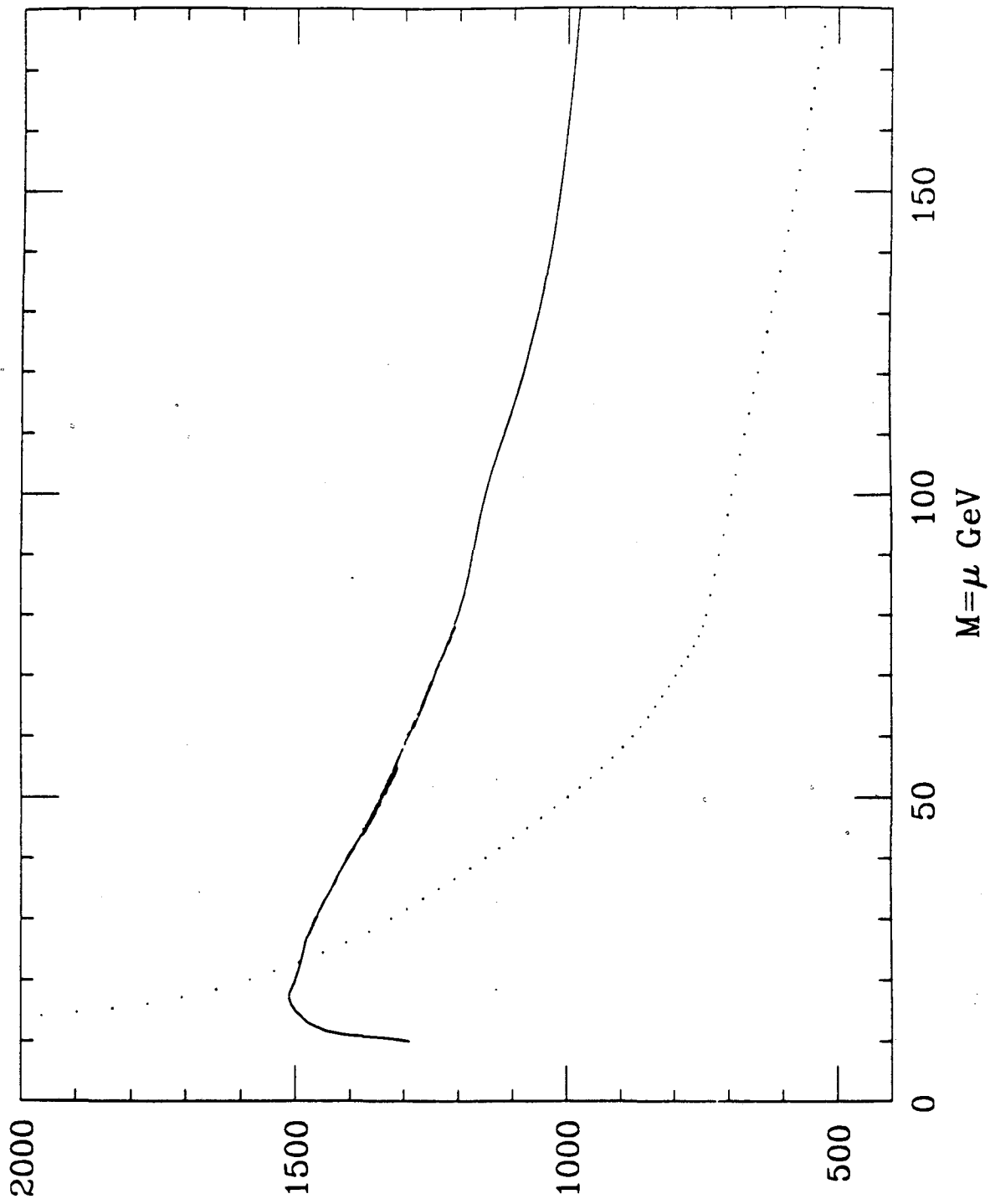

Figure 14

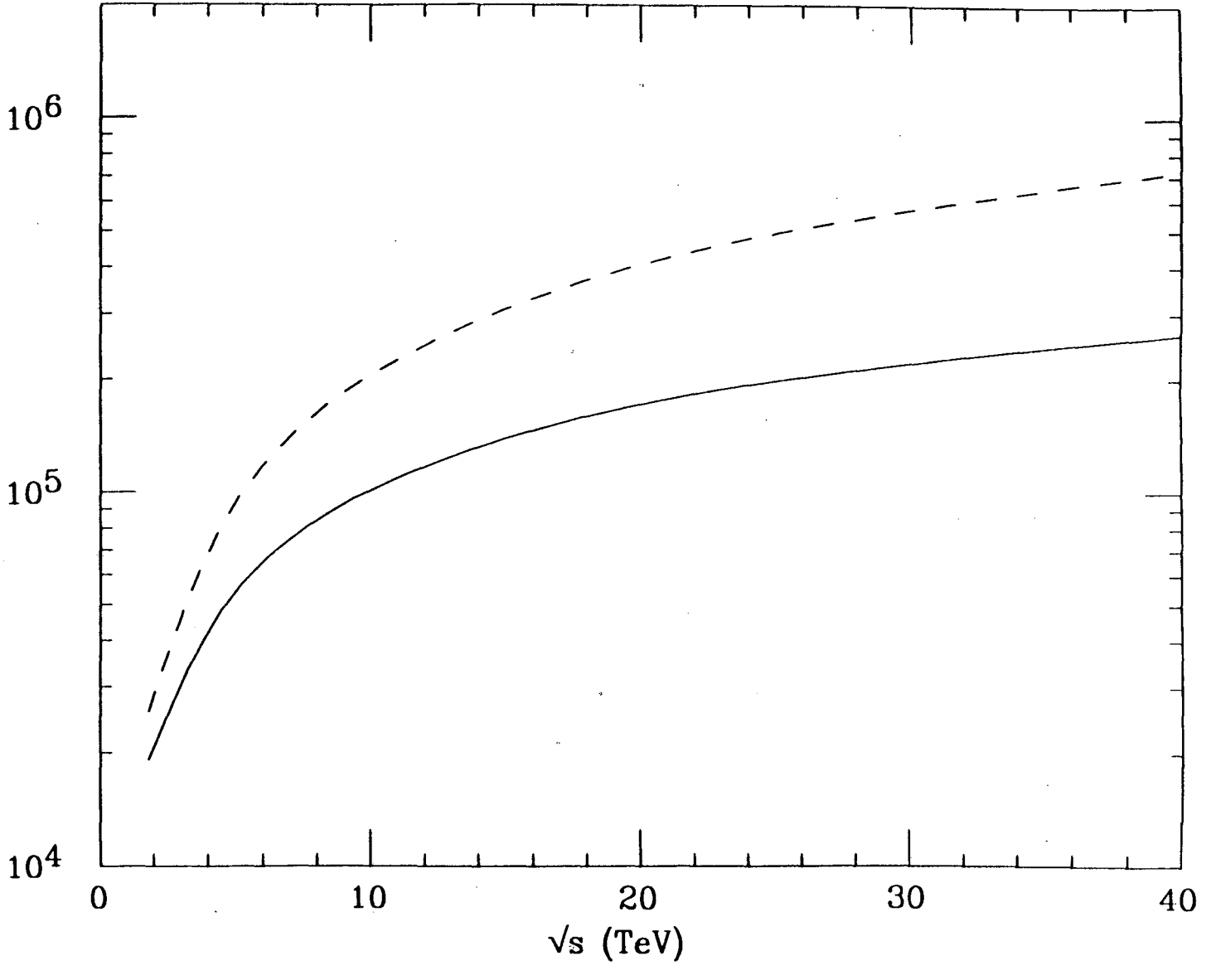

Figure 15

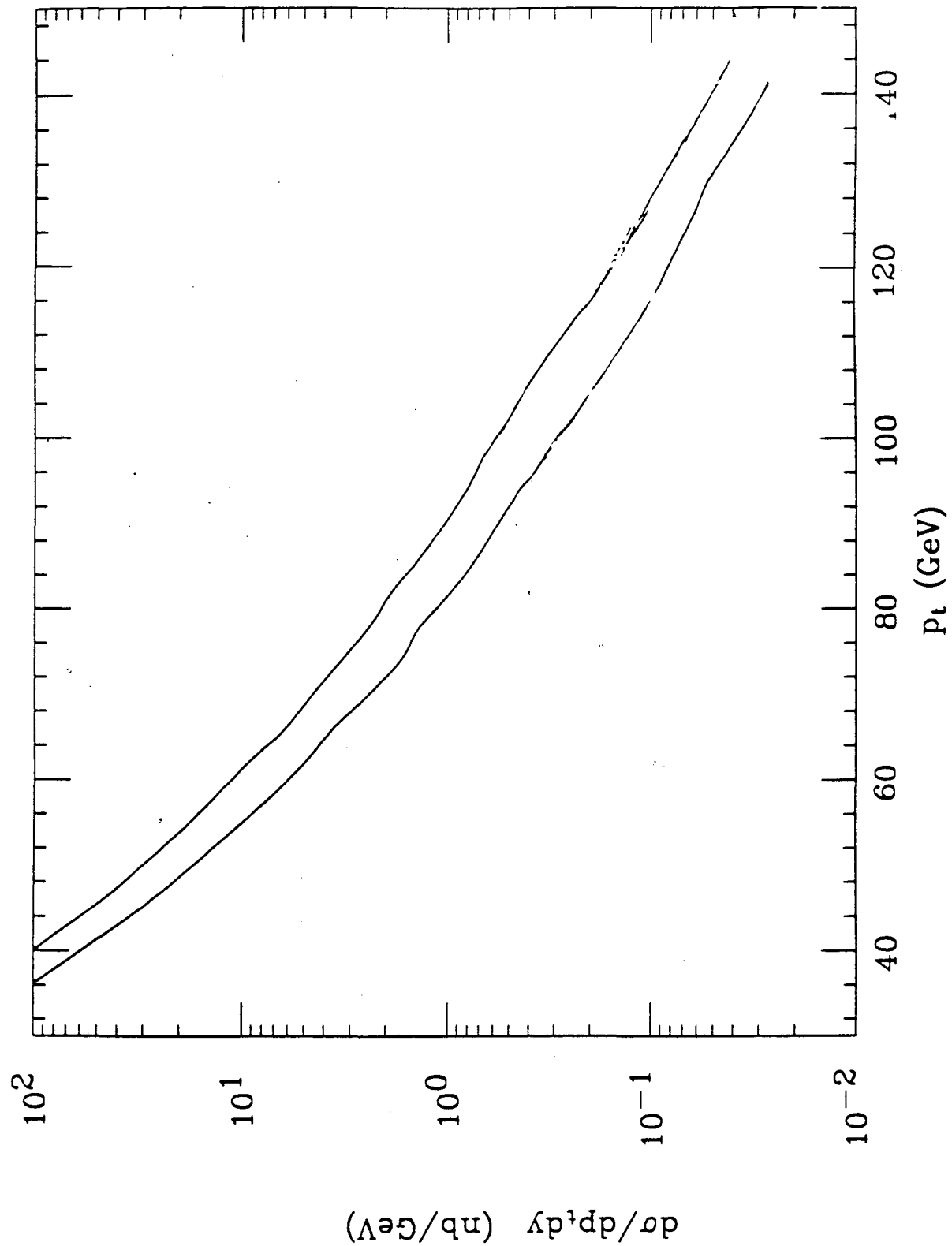
10^2
10^1
10^0
10^{-1}
10^{-2}
$d\sigma/dp_t dy$ (nb/GeV)
40
60
80
100
120
140
p_t (GeV)

Figure 16

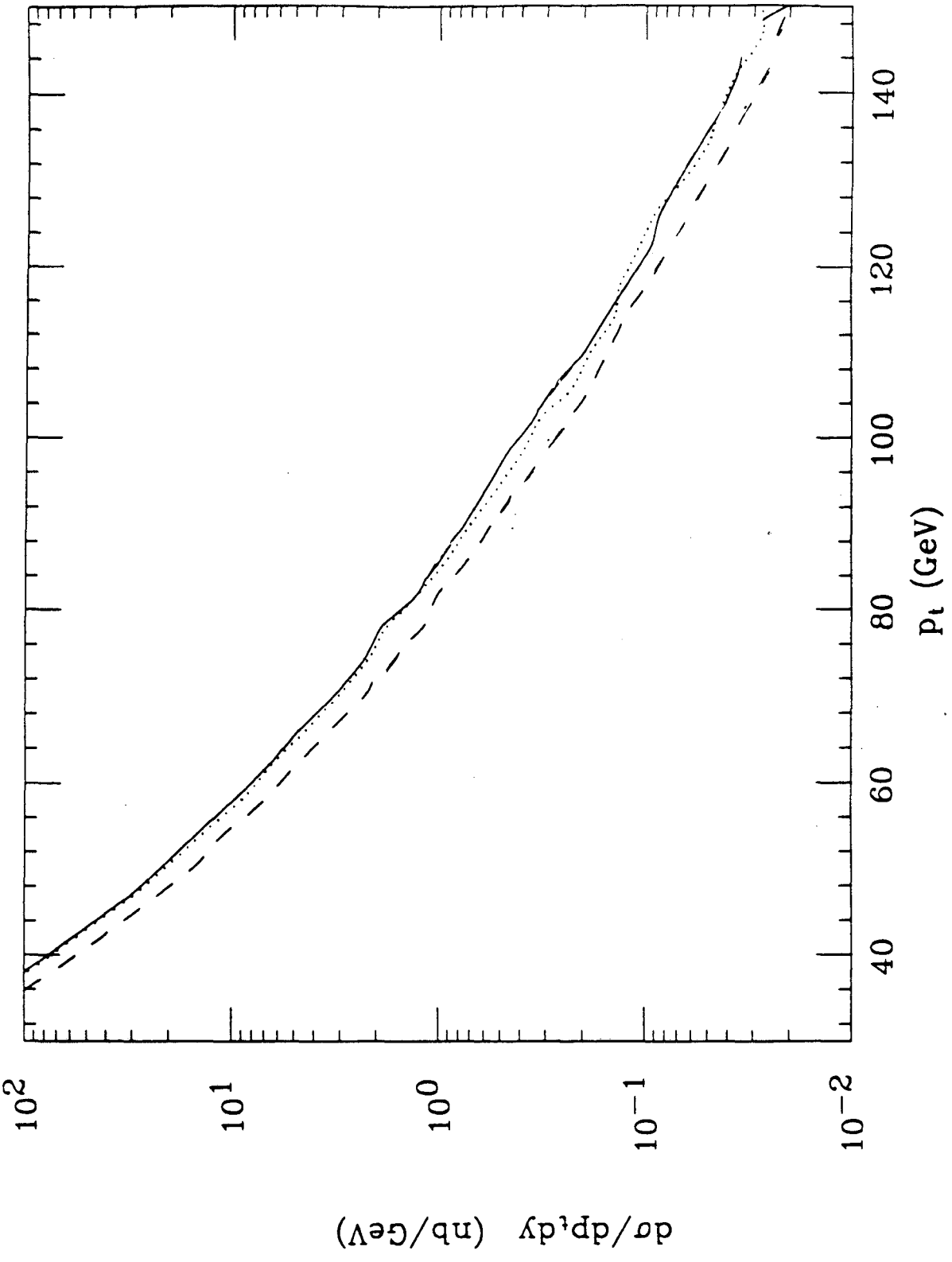
10^2
10^1
10^0
10^{-1}
10^{-2}
$d\sigma/dp_t dy$ (nb/GeV)
40
60
80
100
120
140
p_t (GeV)

Figure 17

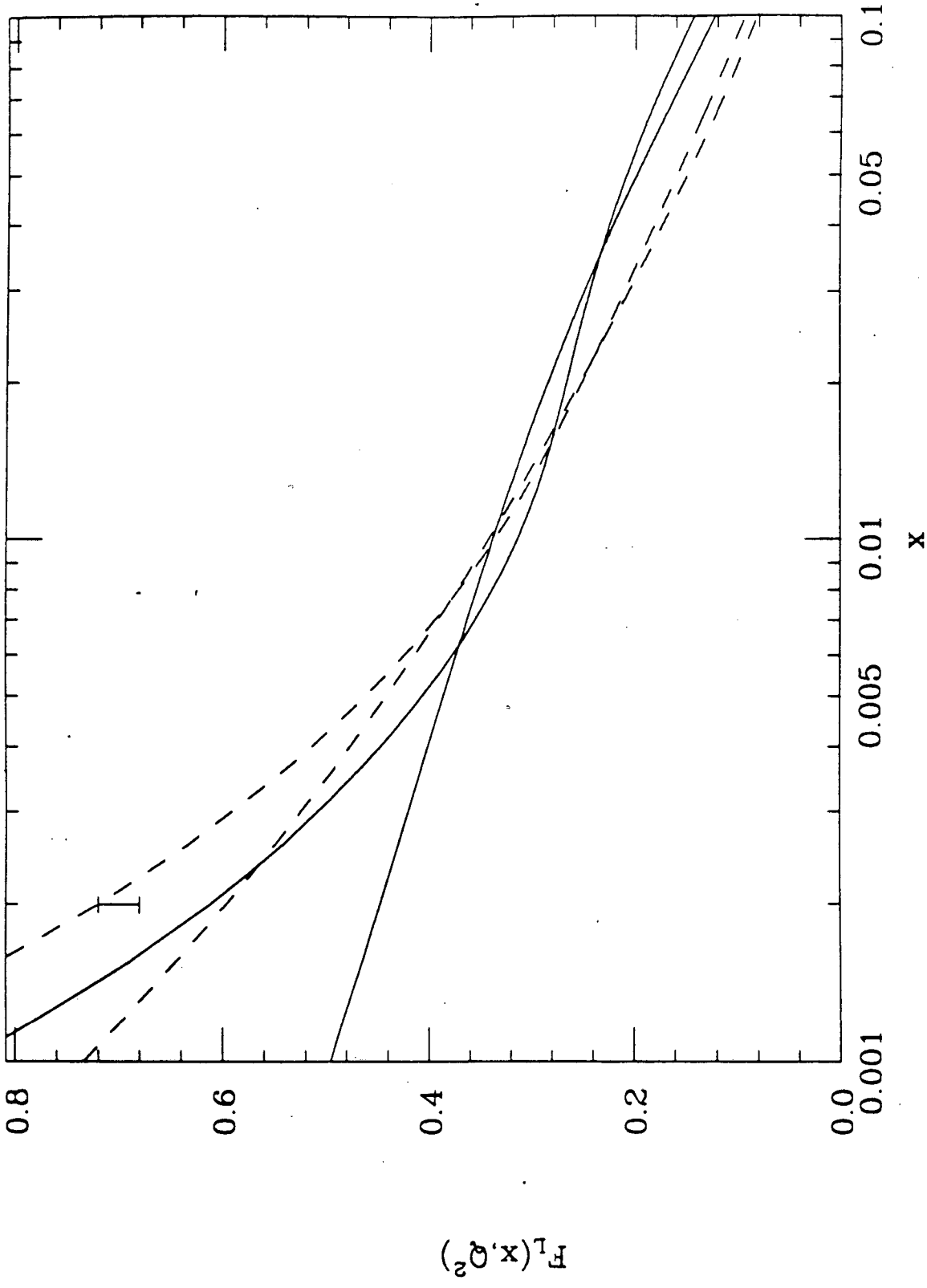

	$m_t = 50$	$m_t = 80$
$EHLQ1$	2.3	0.22
$EHLQ2$	2.0	0.19
$DO1$	2.0	0.20
$DO2$	1.3	0.16
$DFLM(160)$	2.0	0.20
$DFLM(260)$	1.8	0.18
$DFLM(360)$	1.6	0.16
$MRS(EMC)$	2.0	0.20
$MRS(BCDMS)$	2.9	0.41

Table 1.

The total cross-section in nanobarns for the production of a $t\bar{t}$ pair in $p\bar{p}$ collisions at $\sqrt{s} = 1.8\ TeV$ for $m_t = 50, 80\ GeV$. The values given by various sets of distribution functions are shown.

LAWRENCE BERKELEY LABORATORY
TECHNICAL INFORMATION DEPARTMENT
1 CYCLOTRON ROAD
BERKELEY, CALIFORNIA 94720